Weakly dispersive hydraulic flows in a contraction — Nonlinear stability analysis

Bernard K. Ee[†] and Simon R. Clarke

School of Mathematical Sciences, Monash University, Victoria 3800, Australia.

[†]*Currently at Department of Mathematics and Statistics, King Fahd University of Petroleum and Minerals, KFUPM PO Box 5046, Dhahran 31261, Kingdom of Saudi Arabia*

Abstract

The nonlinear stability of steady weakly dispersive hydraulic solutions of the forced Korteweg de-Vries equation is investigated here. For numerical convenience the solutions are considered as periodic pairs consisting of an upward and downward jump. Two types of instability are found to occur. For largely symmetric problems, a solitary wave type instability dominates which features subexponential growth prior to saturation. For asymmetric solutions, the downward jump is destabilized by a hydraulic instability in which superexponential growth occurs prior to saturation. A qualitative description of both instability processes is presented using wave kinematics.

Key words: Forced KdV equation, Nonlinear stability, Hydraulic solutions
PACS: 47.35.Bb, 47.35.Fg

1 Introduction

In this paper, we consider the resonant flow of a stratified fluid through a contraction, assuming that the oncoming fluid velocity and width of the contraction are dependent on height. The governing equation for the amplitude, $B(x, \tau)$, of the internal wave generated is the forced Korteweg-de Vries (fKdV) equation [1]:

$$B_\tau + \Delta B_x + 6BB_x + B_{xxx} = -\gamma f_x, \tag{1}$$

where x, τ are the along–channel spatial and time coordinates respectively, Δ is a de-tuning parameter quantifying the difference between the flow velocity and the long wave speed and γ is the coefficient of the forcing term $f(x - x_p)$, where $f(0) = 1$ is the peak of the forcing. Then the upstream region is given by $x > x_p$ and the downstream region given by $x < x_p$. The fKdV equation
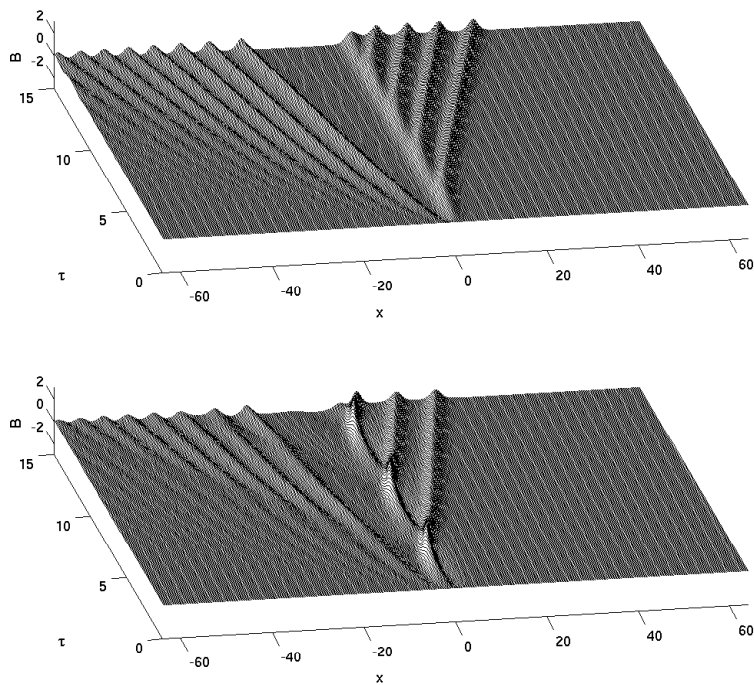
Fig. 1. Numerical solution of (1) for $f = \mathrm{sech}^2 x$ with $\Delta = 0$, and, top panel: $\gamma = 1$, bottom panel: $\gamma = -1$.

also arises in the context of water waves in a channel [2–5], interfacial waves in a shallow fluid [6] and inertial waves in a tube [7] among others.

Of interest here are weakly dispersive hydraulic solutions of the fKdV equation, as previously considered in Grimshaw & Smyth [9] and Ee & Clarke [8]. Weakly dispersive hydraulic solutions consist of hydraulic transitions or jumps which smoothly match an asymptotically flat upstream subcritical state with a similar downstream supercritical state. In Grimshaw & Smyth [9], the solutions of the fKdV equation for a bell-shaped forcing and trivial initial condition were considered. For $\gamma > 0$, it was shown that near-resonant asymptotic solutions consisted of hydraulic transitions connecting upstream solitary wave-trains and a downstream plateau or steady downstream lee waves with an upstream plateau. On the other hand for $\gamma < 0$, unsteady hydraulic transitions were observed. For γ of either sign, asymmetric supercritical and subcritical solutions were obtained outside of the near-resonant regimes. Steady and unsteady hydraulic transitions are illustrated in Figure 1, whereas the (Δ, γ) combinations which describe the various flow regimes are given in Figure 2 for a typical bell-shaped forcing.

In Ee & Clarke [8], a family of weakly dispersive steady hydraulic periodic solutions and their corresponding linear stability were considered. Let the upstream and downstream height of a weakly dispersive hydraulic solution be respectively A_+ and A_-. Then for $A_+ > A_-$, the transition is defined as an
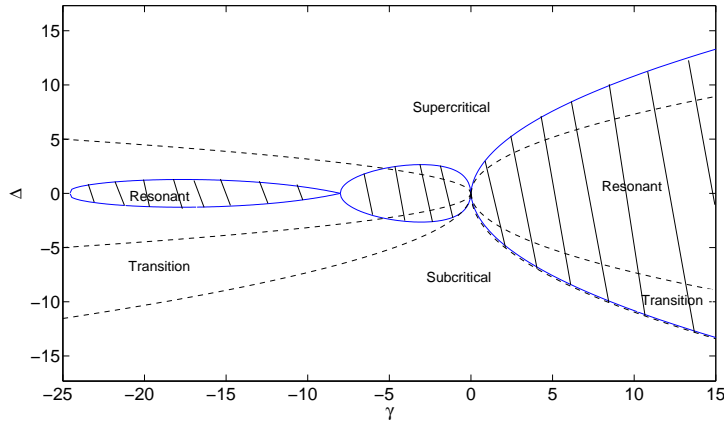
Fig. 2. The parameter space for solutions of (1) for $f = \mathrm{sech}^2 x$. The dashed lines and text denote denote asymptotic regimes for the solutions of (1) for the trivial initial condition. The solid lines and shading depict allowable boundaries for the dispersive hydraulic solutions considered here.

upward jump and for $A_+ < A_-$ as a downward jump. Due to the symmetry of the fKdV equation, periodic hydraulic solutions over an interval $[0, x_u]$ can be constructed with an upward jump centered at $x_p = 3x_u/4$ and its reflected downward jump centered at $x_p = x_u/4$. The periodicity of these solutions over large domains allows Fourier methods for be used to investigate the linear and nonlinear stability. A continuous spectrum of these steady hydraulic solutions were obtained for which the parameter space is shown in Figure 2. The dashed lines in this figure were obtained from numerical experimentation and the asymptotic behaviour of Grimshaw & Smyth [9] that regime boundaries must behave as $\Delta = O(|\gamma|^{\frac{1}{2}})$ for $|\gamma| \gg 1$. The solid boundaries are obtained by using the numerically obtained parametric relationship of Ee & Clarke [8], subject to the restriction that the downstream amplitude must be negative and the upstream amplitude must be positive.

For $\gamma > 0$, these upward jump solutions extend the limits used by Grimshaw & Smyth [9] to construct asymptotic solutions to the trivial initial value problem for the fKdV equation. It was shown that the upward jump solutions, being monotonic, were linearly and nonlinearly stable whereas the downward jump solutions were linearly unstable. On the other hand for $\gamma < 0$, the jump solutions are non-monotonic and both the upward and downward jumps are generally linearly unstable. These include solitary wave (symmetric) solutions at $\gamma = -8$ and $\gamma \approx -24.5$. No other supercritical or subcritical symmetric solutions were obtained on the branch of solutions documented in Ee & Clarke [8].

The focus of Ee & Clarke [8] was linear stability; here we are interested in the nonlinear stability of the family of solutions obtained in that paper. Previous studies of the nonlinear stability of solutions of (1) have focused on forced

solitary wave solutions. In particular, Camassa and Wu [10] classified the evolution and asymptotic behaviour of the solitary wave solutions to (1) in terms of the eigenvalue spectrum and the size of the de-tuning parameter which were derived from their linear stability analysis. Three regimes are described in that paper, of interest to us is the regime associated with the solitary wave solution with $\Delta = 0$. This regime, their periodic bifurcating regime, matches our definition of the solitary wave solution for $\gamma = $ -8.

The goal of this paper is to investigate the nonlinear stability of the dispersive hydraulic solutions in Ee & Clarke [8]. In doing so, we aim to present a qualitative explanation of the physics of this instability. This seeks to explain not only the isolated and symmetric periodic solutions described earlier but also the instability of periodic solutions generated by pairs of topographic perturbations with differing amplitudes. Such solutions have been considered by Dias and Vanden-Broeck [12] and were discussed in Ee & Clarke [8]. In Sec. 2 we characterize the nonlinear stabilities of the solitary wave and dispersive hydraulic solutions. In Sec. 3 we attempt to explain the nonlinear stability for both these types of instability using conservation principles and wave kinematics.

2   Nonlinear stability characterization

We introduce a perturbation variable $C(x, \tau)$ such that $B(x, \tau) = B_s(x) + C(x, \tau)$ satisfies the original evolution equation (1) and B_s is a periodic steady solution as discussed in Ee & Clarke [8]. Hence:

$$C_\tau + ((\Delta + 6B_s)C)_x + 6CC_x + C_{xxx} = 0, \tag{2}$$

where

$$\Delta_c = \Delta + 6B_s,$$

is referred to as the velocity perturbation.

When considering linear stability, we neglect the nonlinear term $6CC_x$ in (2) and transform the resulting equation into a matrix equation whose solution can be constructed in terms of eigenvalues and eigenfunctions. The instability of a particular solution is characterized by the magnitude of the eigenvalue with the largest real part. We denote this as the leading eigenvalue and the corresponding real part, σ_r. In terms of σ_r, it was shown that all the periodic dispersive hydraulic solutions were weakly linearly unstable. The growth rate, σ_r, is a function not only of γ but also of domain size. For sufficiently large domains, as the domain length is increased the dominant effect on the instability spectrum is to cause a periodic variation in the growth rate at fixed γ. In Figure 3 this variation in σ_r is shown as Δx (grid size) is varied for a
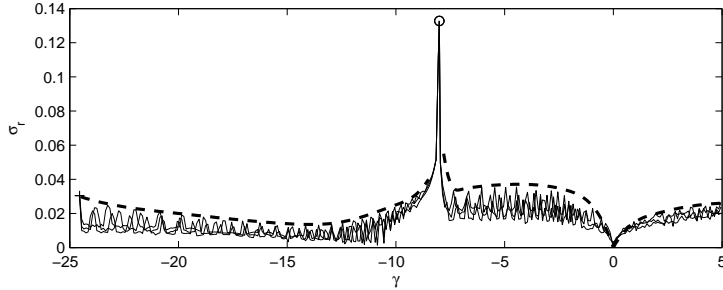
Fig. 3. Plots of the growth rate σ_r for periodic dispersive hydraulic solutions of (1), as a function of γ. The envelopes are formed by solving the matrix stability equation given in Ee & Clarke [8] using $n_u = 1024$, $x_u = 256,\ 204.8,\ 170.6$. The dashed bold line denotes the approximate upper limit of the eigenvalue envelope.

spectral calculation. What is of interest in this figure is the upper limit of the eigenvalue envelope, as this provides for a given value of γ, the maximum asymptotic growth rate of an instability in the vicinity of a particular domain size. As will be seen, this is particularly important when we consider the nonlinear instability of a particular solution.

For a periodic domain, or when $C = C_x = 0$ at the boundaries, the momentum conservation principle for (2) is obtained by multiplying by C and integrating over the domain, whereupon

$$\frac{\partial}{\partial \tau} \int_0^{x_u} \frac{C^2}{2} dx + \int_0^{x_u} \Delta_{cx} \frac{C^2}{2} dx = 0, \tag{3}$$

or

$$\frac{\partial I_1}{\partial \tau} + I_2 = 0.$$

The integral I_2 is a particularly useful quantity as it allows growth of instabilities to be isolated to within the vicinity of variations in the velocity perturbation. In particular for a periodic dispersive hydraulic solution consisting of an upward and downward pair of jumps, we can write

$$I_2 = \int_0^{x_u/2} \Delta_{cx} \frac{C^2}{2} dx + \int_{x_u/2}^{x_u} \Delta_{cx} \frac{C^2}{2} dx = I_2^d + I_2^u.$$

Each separate term then quantifies the growth of instabilities associated with either the downward or upward jump. As will become apparent, this is useful in the characterization of instabilities and allows us to use a sufficiently large domain as a proxy for an infinite domain.

Let

$$\min_x \Delta_{cx} = -\Delta_{cx}^*,$$

then

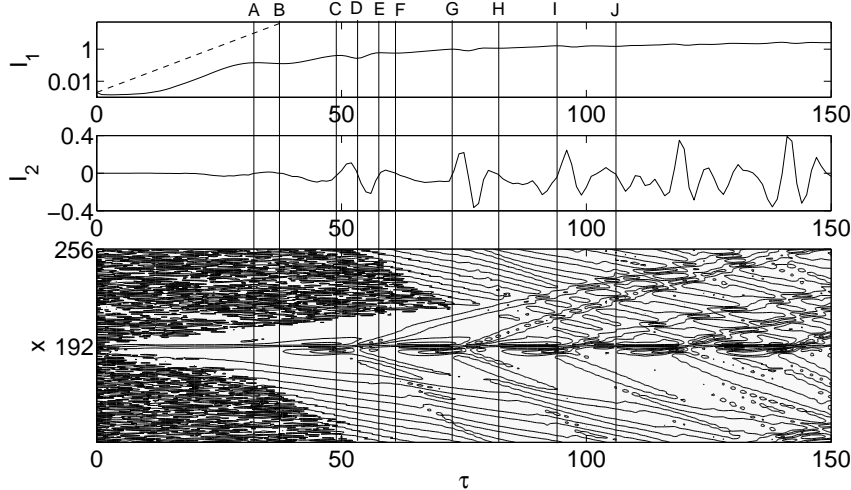$$\frac{dI_1}{d\tau} \leq \Delta_{cx}^* I_1,$$

5

Fig. 4. Nonlinear evolution of a solitary wave type instability for (2). Top panel: Semilog plot of perturbation momentum vs time. Middle panel: a plot of I_2 vs τ. Bottom panel: a contour plot of the numerical solution of (2). All three plots were obtained for the region $[x_u/2, x_u]$ using $\Delta = 0$, $\gamma = -8$, $x_u = 256$, $n_u = 1024$. Initial condition was a random field bounded between $[-0.01, 0.01]$. Dotted line in top panel refers to the growth associated with $\sigma_r = 0.13275$.

from (3). This leads us to determine an upper bound for I_1:

$$I_1(\tau) \leq I_1(0)e^{\Delta^*_{cx}\tau}.$$

Hence as shown in Ee & Clarke [8], the upward jump solutions for $\gamma > 0$ are linearly and nonlinearly stable.

2.1 Solitary wave instability

As in Ee & Clarke [8], the initial condition used in the numerical simulations is a random field and the simulations are performed using a pseudospectral approach for calculation of spatial derivatives and fourth-order Runge-Kutta time-stepping.

In considering the instability of the solitary wave solution for $\gamma = -8$, since the solution is symmetric, we need only consider half of the domain given by $[x_u/2, x_u]$. Figure 4 shows the evolution of I_1 and I_2 in the top and middle panels, together with a contour plot of the perturbation variable, C, in the bottom panel.

The initial growth regime for the instability is that of linear growth where $I_1 \sim e^{2\sigma_r t}$ and in this case, $\sigma_r = 0.13275$. This value of σ_r corresponds to the growth rate of the linear perturbation momentum for the given γ, n_u and Δx. This regime lasts until the first local minima in I_2, just prior to the point A

6

shown in the figure. Immediately following this regime, I_1 continues to grow, albeit at a slower rate than the linear growth rate until the first local maxima in I_1 is encountered at point A. Thus the first effect of nonlinearity in this case is to cause sub-exponential growth up to the first saturation point at A. From (3), it is clear that the growth of instabilities require $I_2 < 0$. Thus instabilities must be generated in this process along the upstream flank on the forced solitary wave, i.e. $x \in [3x_u/4, x_u]$.

In the regime marked by AB, a decrease in I_1 to a local minima at B is observed. Thus $I_2 > 0$ for this period which could be due to two possible scenarios. Either there is preferential growth of instabilities on the downstream flank of the topography or the instabilities which previously formed on the upstream side form a coherent structure which then self-advects upstream. From the lower panel of Figure 4, it appears that it is the latter scenario which occurs although the structure is not observable far upstream.

Then in the region BC the process observed to A is largely repeated. Again, I_2 in this region is negative definite, indicating preferential growth of the instability on the upstream flank of the topographic perturbation. However, this does not preclude growth on the downstream sides. Instead, the contour plot suggests the growth of long waves on the downstream side and shorter waves on the upstream side. At the saturation point C for I_1, it appears that the downstream long waves propagate upstream and eventually away from the topography. The energy conservation principle for (2):

$$\frac{d}{d\tau} \int_0^{x_u} C dx = 0,$$

requires the downstream propagation of energy which appears to occur here in the form of a nonlinear wave group. This propagation of a small amplitude solitary wave upstream and a nonlinear wave group downstream occurs in the region CD. Note the amplitude of these upstream propagating solitary waves is significantly smaller than that of the original forced solitary wave. From D, this process is repeated leading to the formation and upstream propagation of a second solitary wave at G and subsequently, a third one at I. Asymptotically, the wrap-around propagation of instabilities leads to a sea of turbulence throughout the domain where the input of momentum at the topographic perturbation is balanced due to numerical dissipation.

Qualitatively, the features described here are in agreement with that of Camassa and Wu [10]. Rather than the random field used here, the instability described in Camassa and Wu [10] was initialized using a coherent structure localized to the region of the forced solitary wave.
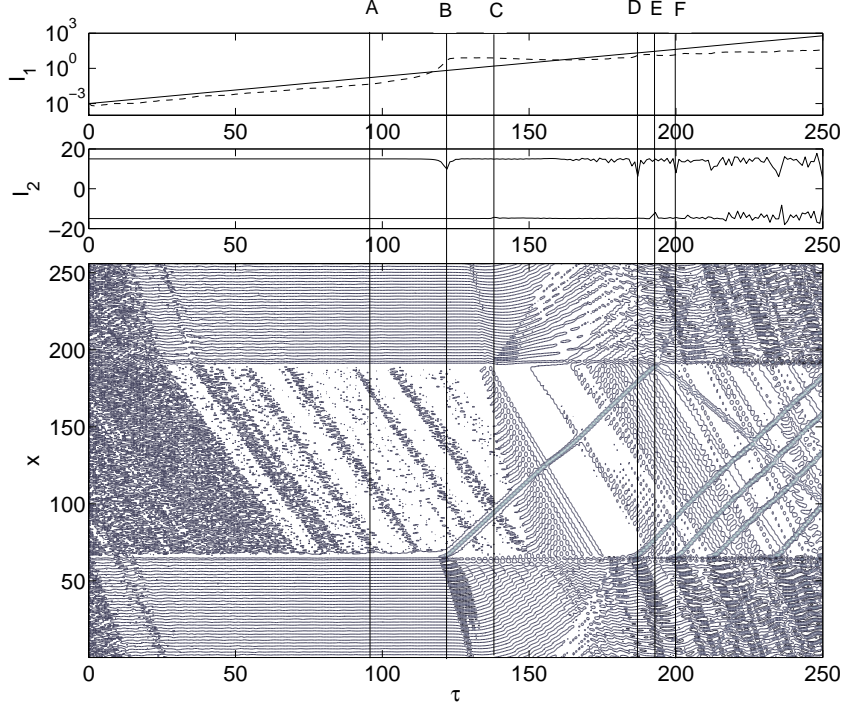
Fig. 5. Nonlinear evolution of a hydraulic type instability for (2). Top panel: Semilog plot of perturbation momentum vs time where dominant eigenvalue is $Re(\overline{\sigma}_{max}(\gamma)) = 0.02661$ (dashed line). Middle panel: Plots of I_2 vs τ over the original (translated down) and reflected (translated up) regions. Bottom panel: a contour plot of the numerical solution of (2). All three plots were obtained using $\gamma = -2.55$, $x_u = 256$, $n_u = 1024$. Initial condition was a random field bounded between $[-0.01, 0.01]$.

2.2 Hydraulic instability

For γ sufficiently larger than -8 the nature of the instability of the steady forced asymmetric solutions of Figure 2 is qualitatively different from the solitary wave instability described in the last section. We will refer to this type of instability as hydraulic instability. For one, the periodic solution involves an upstream jump in $[x_u/2, x_u]$ and a downstream jump in $[0, x_u/2]$ which each have different instability characteristics. To characterize the instability associated with each of these regions, we can consider the contributions to I_2 from the upstream and downstream regions, denoted as I_2^u and I_2^d respectively.

A representative example of hydraulic instability is shown in Figure 5. Turning to the top panel of this figure, it is again useful to divide the evolution into regions based on the behaviour of I_1. The first of these is from $\tau = 0$ to $\tau = 96$ (given by point A), where I_1 experiences linear exponential growth in accordance with the growth rate obtained from the upper limit of the eigenvalue envelope for $\gamma = -2.55$.

8

Subsequently in region AB, we have super-exponential growth which features a nonlinear growth that exceeds the linear exponential growth rate. This region occurs for $\tau \in [96, 122]$. The super-exponential growth regime ends at B which corresponds to an inflection point for I_1 and a local minima for I_2. At this point, saturation of nonlinear effects occurs. As is clear from I_2^d, this nonlinear saturation is purely due to growth at the downstream jump. As a result, a solitary wave and associated nonlinear wave group are observed to propagate away from the downward jump at B. From this inflection point B, the super-exponential growth rate starts to decrease until we encounter a local maxima, or saturation point, at $\tau \approx 124$.

In Figure 5, I_2^u and I_2^d are shown for this case. Again, instabilities must form on the upstream flank of the topography; however in this case, it is apparent that it is the long wave instability which forms on the upstream flank and develops into an upstream propagating solitary wave. Consequently, the instability process is much simpler than the see-saw process on the upstream and downstream flanks which occurs for the solitary wave instability. Here, nonlinear and linear growth are coherent leading to a super-exponential growth regime prior to saturation.

At the point C, we encounter a local maxima in I_2, albeit a small one, giving another inflection point in I_1. This occurs only in I_2^u and is a result of the initial downstream dispersive waves from the reflected topography being wrapped around to the original region and then propagating towards the original topography. Such signals we refer to here as secondary instabilities. An example of this due to a forward propagating solitary wave generated from the downstream jump occurs at E. Subsequent local minima in I_2, given by points D and F, correspond to primary instabilities generated from the reflected topography. The process which occurs appears to be a repeat of the generation of a solitary wave which occurs at B.

2.2.1 Effects of domain variation and initial condition

In Figure 6, we first focus on the effect of variation of the domain size on the evolution of the hydraulic instability. This is achieved by varying either Δx or n_u.

We first consider the effect of keeping Δx fixed, in this case to a value of $1/4$ and varying n_u from 512 to 1024. For the smaller domain, the most obvious difference is that a significantly larger time is required before the asymptotic linear growth regime occurs. However once this occurs, the linear growth rate is approximately equal to that for the larger domain. Similarly, the magnitude of I_1 at saturation is 7.6 ($n_u = 512$) and 7.9 ($n_u = 1024$).

If n_u is fixed to 1024 and Δx is varied from 0.25 to 0.2, then the evolution
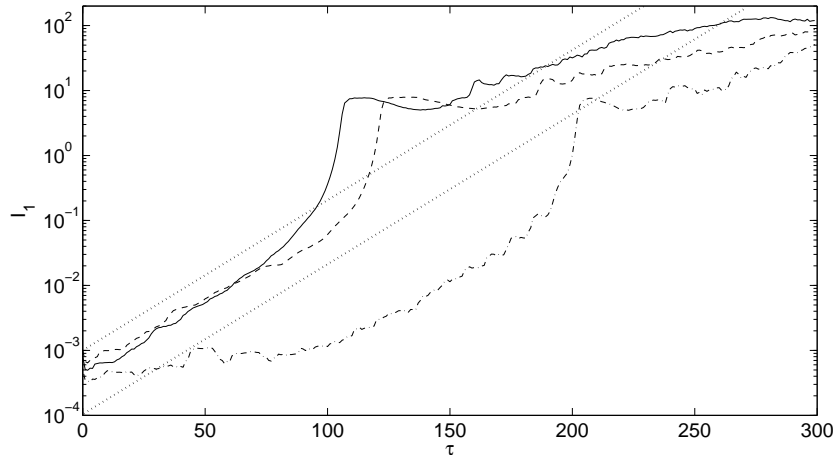
Fig. 6. Nonlinear evolution of a hydraulic type instability for (2). Semilog plots of perturbation momentum vs time for solutions of (2) over combined region using $\gamma = -2.55$ and random field initial condition. The various lines show $\Delta x = 1/5, n_u = 1024$ (bold line), $\Delta x = 1/4, n_u = 1024$ (dashed line), $\Delta x = 1/4, n_u = 512$ (dash-dot line) and linear exponential growth using $Re(\overline{\sigma}_{max}(\gamma)) = 0.02661$ for $\Delta x = 0.24$ (dotted lines).

of I_1 is almost identical except that super-exponential growth commences at slightly earlier time and smaller value of I_1. Both have a dominant growth rate of $\sigma_r = 0.026$ although the linear stability gives $\sigma_r \approx 0.015$ ($\Delta x = 0.25$) and $\sigma_r \approx 0.024$ ($\Delta x = 0.2$).

This phenomena of growth at the dominant rate in the vicinity of a particular domain size only occurs with the random initial condition. If we initialize a simulation with the dominant eigenfunction from the linear stability analysis, the nonlinear simulations demonstrate that the linear growth rate prior to saturation is the theoretical growth rate rather the upper limit of the eigenvalue envelope of Figure 3(b). It would appear resonance between the dominant mode and subdominant modes allows linear growth at the upper limit of the eigenvalue envelope. At saturation and afterwards, similar behaviour occurs with initialization using the dominant eigenfunction as for a random initial condition. Thus for large domains the nonlinear growth is largely independent of domain size, as the growth is localized to the vicinity of the topographic perturbation.

2.2.2 Effect of similar Δ

In Figures 7 and 8, the effect of γ on the nonlinear stability of dispersive hydraulic solutions is investigated. The two steady solutions use almost identical values of Δ but values of γ of opposite sign. Hence for $\gamma > 0$, the jumps are monotonic while for $\gamma < 0$, they are non-monotonic. Furthermore, the value of
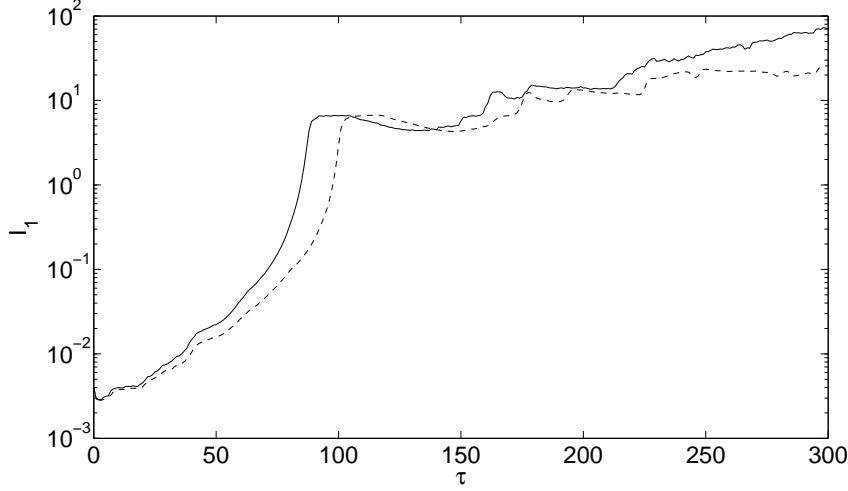
Fig. 7. Evolution of perturbation momentum for hydraulic type instabilities of (2) vs time over combined region with $\gamma = -1.35, \Delta = 2.3362$ (bold) and $\gamma = 0.55, \Delta = 2.34$ (dashed).
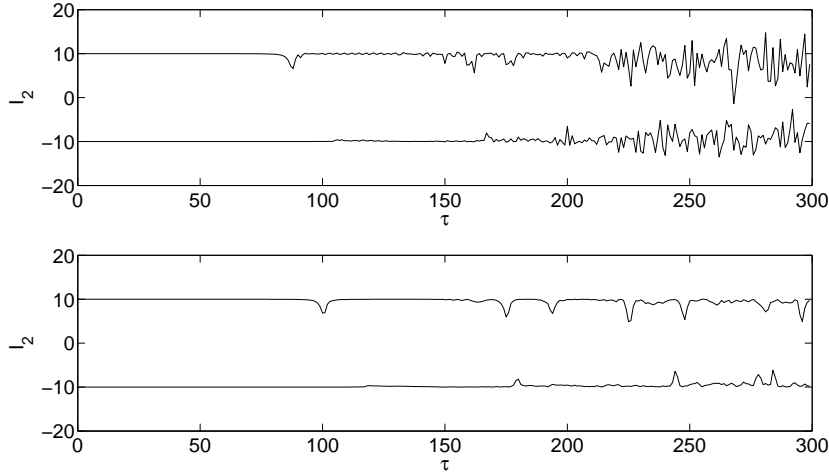

Fig. 8. Evolution of I_2 vs τ for hydraulic type instabilities of (2) over the original (translated down) and reflected (translated up) region. Top panel: $\gamma = -1.35, \Delta = 2.3362$ and bottom panel: $\gamma = 0.55, \Delta = 2.34$. Both employ $x_u = 256$ and $n_u = 1024$.

σ_r, i.e. the linear growth rate, is larger for negative γ solution. Consequently in Figure 7, we observe that the main difference between the two solutions is that the time at which nonlinear saturation occurs is less for $\gamma < 0$ than for $\gamma > 0$.

However the super-exponential growth phase is almost identical for both solutions. In particular the magnitude of I_1 at saturation is 6.62 for both. Thus, we can conclude that it is the value of Δ, which governs the height upstream and downstream of the jumps, that controls the magnitude of the upstream
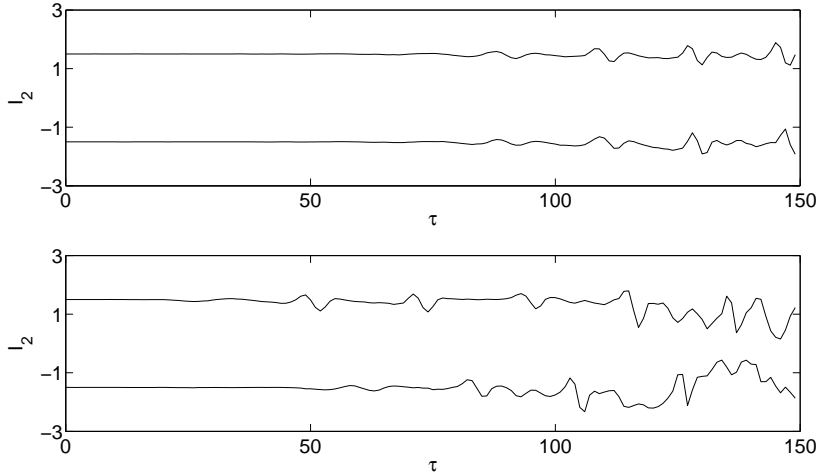
11

Fig. 9. Evolution of I_2 vs τ for solitary wave type instabilities of (2) over the original (translated down) and reflected (translated up) regions for top panel: $\gamma = -8.23$ where there is a symmetric contribution towards the overall instability and bottom panel: $\gamma = -7.992$ with first peak indicating the initial onset of instability due to forcing in reflected region.

propagating solitary waves generated by the hydraulic instability process.

For $\gamma > 0$ since the jumps are monotonic then we must have $I_2^d < 0$ and $I_2^u > 0$. Thus any decrease in I_1 is due to the damping of instabilities propagating through the upstream jump. Figure 8 demonstrates that for $\gamma < 0$, the same behaviour is observed for $\tau \leq 200$. Thus the downstream jump acts as a source of instabilities and the upstream jump acts as an effective sink of instabilities. At later times, this no longer holds. The cause of this would appear to be a slow growth of a solitary wave type instability at the upstream jump.

2.2.3 Instability bands

The simulations with similar Δ demonstrate that for $\gamma > 0$ only hydraulic instability occurs, while for $\gamma < 0$ a mixture of hydraulic and solitary wave instability occur. The rate of each of these two types of instabilities is then dependent on the particular solution, and ultimately γ. For example at $\gamma = -8$ and approximately -24.5, the solutions are symmetric and only solitary wave instability can occur. The form of the instability near $\gamma = -8$ is shown in Figure 9.

In the upper panel, it is apparent that the behaviour upstream and downstream is similar, being characteristic of the solitary wave instability. The downstream instability precedes the upstream instability slightly. In the lower panel, the asymmetry between the two regions is now much more apparent but both the upstream and downstream regions still, at least initially, display
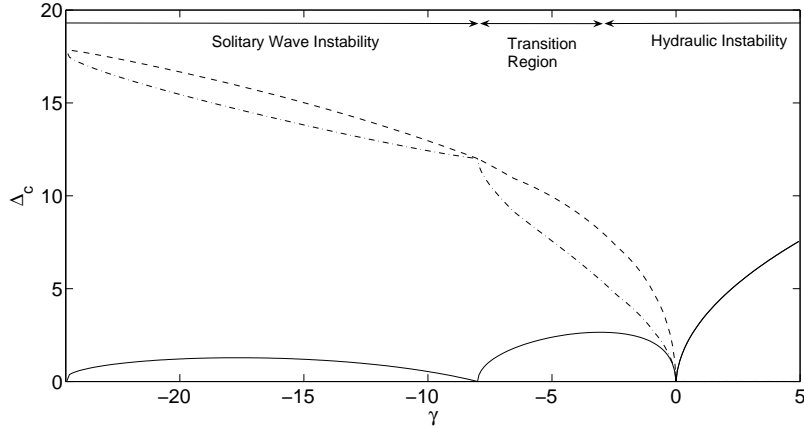
12

Fig. 10. Plot of Δ_c^{max} vs γ (dash), $-\Delta_c^{min}$ vs γ (solid) and $\Delta_c^{max} + \Delta_c^{min}$ vs γ (dash-dot) for $-24.5 \le \gamma \le 5$ for periodic dispersive hydraulic solutions of (1). For $\gamma > 0$, $\Delta_c^{max} = -\Delta_c^{min}$. The corresponding stability regions of solutions of (2) are shown at the top of the figure. Note that for γ positive $\Delta_c^{min} = 0$ and the other two curves coincide.

the characteristic solitary wave type instability. The most significant difference between the two solutions is the value of Δ, which in this case primarily determines the magnitude of the trough and plateau that occurs between the two solitary wave perturbations. Thus we can conclude that an upstream plateau and downstream trough decreases the rate of solitary wave instability, while an upstream trough and downstream plateau increases the rate of the instability.

The solutions being considered here can be characterized in terms of the velocity perturbation $\Delta_c = \Delta + 6B_s$ and can be qualitatively described as consisting of a jump from Δ to $-\Delta$ and for $\gamma < 0$, a localized positive perturbation. For a particular γ, the two main parameters which characterize the solution are therefore Δ_c^{max} and $-\Delta_c^{min}$, each of which can be related to the two types of instability.

Firstly, the rate at which the hydraulic instability occurs would be expected to be dependent on $-\Delta_c^{min}$, whereas the rate at which the solitary wave instability occurs would be expected to be dependent on $\Delta_c^{max} + \Delta_c^{min}$. These two parameters are plotted in Figure 10 as a function of γ. For $\gamma > 0$, $\Delta_c^{max} + \Delta_c^{min} = 0$ and no solitary wave instability occurs. For $\gamma \approx -8$ and $-\Delta_c^{min} \approx 0$, solitary wave instability dominates.

Hence, we could expect that hydraulic instability dominates when $-\Delta_c^{min} \gg \Delta_c^{max} + \Delta_c^{min}$ and solitary wave instability dominates when $-\Delta_c^{min} \ll \Delta_c^{max} + \Delta_c^{min}$. Naturally, we would expect that a transition between the two types of instability occurs in the region $-8 < \gamma < 0$, $\Delta_c^{max} \approx -2\Delta_c^{min}$. For $\gamma < -8$, $\Delta_c^{max} \gg -2\Delta_c^{min}$ and so we would expect the solitary wave instability to

13

dominate.

3 Nonlinear stability analysis

In this section we develop using the theory of wave kinematics a qualitative description of the instability processes numerically documented in the previous section. In particular, this aims to address four points.

(1) Why the rate of instability is greater for non-monotonic jumps than for monotonic jumps with the same values of Δ.
(2) That for large domains, the rate of instability is independent of domain size.
(3) Why the initial nonlinear growth phase for hydraulic instability is super-exponential.
(4) Why an upstream trough and downstream plateau decrease the rate of solitary wave instability and increases the rate when the upstream and downstream conditions are reversed.

To understand the nature of the instability process, we use the averaged variational or wave kinematics approach of Whitham [13]. For a slowly varying wavetrain with amplitude a and wavenumber, k, then in the linear limit the wavenumber is advected along rays such that

$$\frac{dk}{d\tau} = -W_x \quad \text{on} \quad \frac{dx}{d\tau} = V$$

where

$$W = \Delta_c k - k^3 \tag{4}$$

is the local dispersion relationship and

$$V = W'(k) = \Delta_c - 3k^2 \tag{5}$$

is the local group velocity. The subscript x denotes here explicit differentiation with respect to x. Since the system is time invariant, the energy density is defined to be

$$\mathcal{E} = \frac{W a^2}{k}$$

and advected along rays according to

$$\frac{d\mathcal{E}}{d\tau} = -V_x \mathcal{E} \quad \text{on} \quad \frac{dx}{d\tau} = V.$$

14

Along a ray the above equations imply that a wave group conserves its frequency, (4), and the energy density flux

$$V\mathcal{E} = \frac{(\Delta_c - 3k^2)Wa^2}{k}$$

which determines the wavenumber, $k = k(\tau, x_0)$ and amplitude $a = a(\tau, x_0)$, where x_0 is the initial position of the ray. Alternatively as the ray is defined as $x(\tau)$, $k = k(x, x_0)$ and $a = a(x, x_0)$. Asymptotically the behaviour will be independent of the initial position of the ray, in which case $k = k(x)$ and $a = a(x)$. This asymptotic behaviour is also referred to as steady propagation of the wave group.

Furthermore, Whitham [13] showed that for the KdV equation, the weakly nonlinear group velocities bifurcate and the amplitude propagates along

$$V_a = V + \frac{3a}{k} \tag{6}$$

while the wavenumber propagates along

$$V_k = V - \frac{3a}{k}. \tag{7}$$

Note that this differs from the corresponding expressions in Whitham[13], as there the amplitude of $\int C\ dx$ is used.

In the limit of steady propagation of the wave group, conservation of frequency results in the following relationship between velocity and wave number:

$$\Delta_c = \frac{W + k^3}{k}. \tag{8}$$

Assuming that $k > 0$ without loss of generality, the curves that result are shown in Figure 11. The behaviour that results then depends on which branch the solution lies upon. For a fixed $\Delta_c > 0$, the three branches correspond to long waves (Branch I, $k \leq (\Delta_c/3)^{1/2}$), intermediate waves (Branch II, $(\Delta_c/3)^{1/2} \leq k \leq \Delta_c^{1/2}$) and short waves (Branch III, $k \geq \Delta_c^{1/2}$).

Since frequency is constant, conservation of energy density requires Va^2/k is constant, or

$$\frac{d}{dx}(\ln\ a^2) = -\frac{1}{V}\frac{dV}{dx} + \frac{1}{k}\frac{dk}{dx}. \tag{9}$$

Given W is constant , then

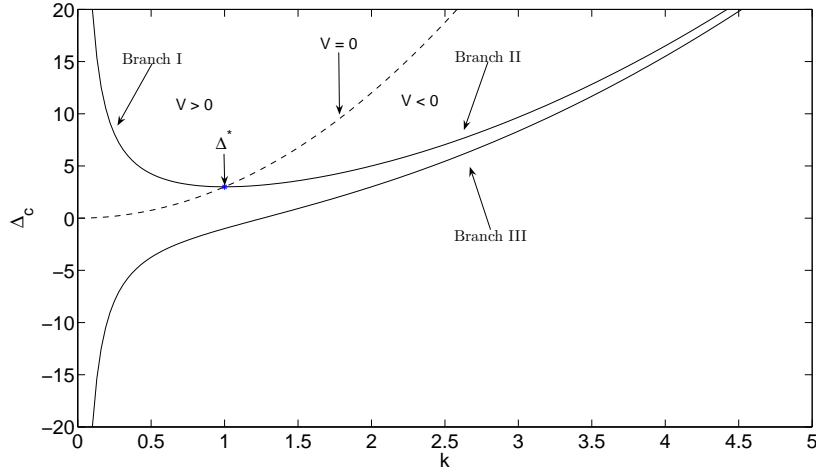$$\frac{1}{k}\frac{dk}{dx} = -\frac{\Delta_{cx}}{V}, \tag{10}$$

15

Fig. 11. Plots of (8) for $W = 2$ (Branch I - $V > 0$, Branch II - $V < 0$), $V = 0$ (dashed) and $W = -2$ (Branch III).

and consequently

$$\frac{d}{dx}(\ln\ a^2) = -\frac{1}{V}\left(\frac{dV}{dx} + \Delta_{cx}\right). \tag{11}$$

Differentiation of (5) gives $dV/dx = \Delta_{cx} - 6k \times dk/dx$, or using (10)

$$\frac{dV}{dx} = \Delta_{cx} + \frac{6k^2\Delta_{cx}}{V}.$$

Hence the numerator in (11) can be written as

$$\frac{dV}{dx} + \Delta_{cx} = \frac{2\Delta_{cx}}{V}(V + 3k^2) = \frac{2\Delta_{cx}}{V}\Delta_c.$$

This will finally give

$$\frac{d}{dx}(\ln\ a^2) = -\frac{2\Delta_{cx}}{V^2}\Delta_c = -\frac{(\Delta_c^2)_x}{V^2}. \tag{12}$$

Compare (12) with the global conservation law which states that the growth of instabilities can only occur if $\Delta_{cx} < 0$. Here the growth of instabilities is dependent on the change of $|\Delta_c|$. Hence for amplification of a wavegroup in the direction of propagation, $|\Delta|$ must be decreasing.

3.1 Hydraulic Instability

Consider first wavegroups on Branch III. In this case, $V < 0$ and hence energy propagates downstream throughout the domain. If we commence on a trough of a solution at the minimum of Δ_c, then as the wave group propagates downstream, its wavenumber increases until it reaches a maximum on the plateau

16

of the domain. The wavenumber then decreases until the minimum of Δ_c is again reached. The amplitude throughout the domain is given by (13)

$$a^2 = \frac{ka_0^2 V_0}{k_0 V},\tag{13}$$

where k is the wavenumber, V is the local group velocity defined in (5) and k_0, V_0 denote an initial wavenumber and local group velocity. Since $V < 0$, the amplitude a remains bounded. Hence wavegroups of Branch III can be assumed to be stable.

Consider now waves on Branches I and II and let the minimum of Δ_c at the intersection of the two branches be Δ^*. For a wavegroup on Branch II, $V < 0$ and hence the wave must propagate downstream towards Δ^*. In the process, its wavenumber must decrease and amplitude must increase since $V \to 0$ as $\Delta \to \Delta^*$. At Δ^* where $V = 0$, the amplitude obtained from wave kinematics becomes singular, which from linear theory would indicate the presence of a caustic. That is the wavegroup passes through Δ^* onto Branch I, where $V > 0$, and then propagates upstream where its wavenumber and amplitude now both decrease until the minimum in Δ_c is reached. After this point, the progress is down Branch I where the wavenumber and amplitude increase until Δ^* is reached, indicating the presence of an upstream caustic. What the linear simulations in Ee & Clarke [8] demonstrate is that this upstream caustic is unstable whereas the downstream caustic is stable.

Within a caustic the slowly varying and linear assumptions of wave kinematics eventually break down. To determine the effect of the former, consider the rate at which the amplitude increases from (12), in particular

$$V\frac{d}{dx}(\ln \ a^2) = -\left(\frac{dV}{dx} + \Delta_{cx}\right).\tag{14}$$

On Branch I as Δ^* is approached, both terms of the RHS of (14) are positive while on Branch II, $-dV/dx < 0$ but $-\Delta_{cx} > 0$. Thus cancellation of these two terms occurs on Branch II and reinforcement occurs on Branch I. Consequently, the rate of increase would be expected to be faster on Branch I than on Branch II. Hence, the neglected linear terms must balance the amplitude growth on Branch II resulting in stability at the caustic on the upward jump while this is not able to occur at the downward jump resulting in instability at this point. This buildup of energy is radiated away from the caustic on rays which propagate downstream, resulting in an exponentially growing mode.

The above argument has been formulated in terms of an arbitrary upstream wavenumber; however, there would be expected to be a mode for which maximum growth occurs on Branch I as Δ^* is approached. Qualitative arguments would suggest that this is the pair for which the long wave between jumps

has $k \approx 0$ and the shorter wave has $k \approx \Delta_c^{1/2}$. For this pair $\Delta^* \approx 0$ and the extent of the two branches is largest. Hence, the dominant mode would have frequency $W \approx 0$.

For a periodic domain, only discrete wavenumbers are possible. Therefore in general, it would be expected that the growth rate is slightly less than described above as the dominant growth mode has a short wave component for which $k < \Delta^{1/2}$. Thus we obtain the eigenvalue envelope in Figure 3.

Consider now the effect of nonlinearity, using that the energy density propagates along the ray V_a, (6). At the upward jump, the incoming ray has $V < 0$. Consequently, the effect of nonlinearity is to increase V_a and the wavegroup undergoes a turning point more rapidly. At the downward jump, the opposite applies in that the incoming ray has $V > 0$ and so the effect of nonlinearity is to delay the onset of the turning point. Thus nonlinearity enhances the stability at the upward jump and the instability at the downward jump. This has two consequences on instability. Firstly, it would appear to cause enhanced decay of the instability away from the topographic perturbation. Thus for a sufficiently large domain, the instability, even for very small amplitudes, grows at the optimal rate. Secondly, for sufficiently large amplitudes wave groups will have zero velocity at Δ^* and resonance occurs resulting in nonlinear growth occurring at a faster rate than the theoretical linear growth. The result of this is the super-exponential growth observed prior to saturation in the numerical simulations.

3.2   Solitary Wave Instability

For a qualitative description of the solitary wave instability process, the discussion of wave modification on Branches I and II is still relevant except that the change in Δ_c occurs over a localized region and in this case $\Delta_c \geq 0$. Consequently a trapped mode forms over the topographic perturbation with a source of instabilities for short waves on the upstream flank. Since exponential decay is not relevant for a localized mode, we therefore have a corresponding source of instabilities for long waves on the downstream flank. Hence, upstream of the topographic maximum we would expect to observe short waves propagating downstream. On the other hand downstream of the topographic maximum, we would expect to observe long waves propagating upstream. Indeed, this is confirmed by Figure 4 which again suggests that the most unstable mode has $W \approx 0$.

Again to assess the effect of saturation, we can consider the propagation of energy. In this case, the upstream and downstream modifications to V_a due to near linear correction would be expected to cancel each other and so the region

the trapped wave occupies does not change significantly. Consequently, super-exponential growth to saturation would not be expected. Indeed the numerical simulations demonstrate that sub-exponential growth occurs prior to saturation. Thus the initial effect of nonlinearity is to dampen the linear growth as opposed to the hydraulic instability where nonlinearity first enhances the linear growth.

3.3 Mixed Instability

The qualitative description in the previous subsections have concentrated on pure forms of the solutions, i.e. jumps which are monotonic and localized structures which have $\Delta_c = 0$ both upstream and downstream. However this only addresses the region $\gamma > 0$ and the discrete points of $\gamma = -8$ and approximately -24.5 in Figure 2. In general for $\gamma < 0$, the steady jumps are of mixed type. Two limits of these solutions can be considered. For $-5 < \gamma < 0$, the jump structure dominates while for $\gamma < -7$, the localized structure dominates compared to the magnitude of the jumps. The instability of these two limits are discussed in detail below.

When the instability is dominated by a hydraulic instability, at both the upward and downward jumps there now exists the possibility of trapped modes for waves with frequency such that $\Delta^* = \Delta$. Let Δ_m be the maximum of Δ_c over the domain. Hence the rate of growth would be expected to be dependent on $|\Delta_m - \Delta|$. Two consequences result. Firstly, an upward jump would now be expected to be unstable, where the instability is a solitary wave instability, except that the dominant wavenumber has wavelength $k \approx (\Delta/3)^{1/2}$ rather than $k \approx 0$. Secondly, as has been seen previously, the interactions of unstable modes appear to lead to faster growth at earlier stages even for relatively small amplitudes. This would explain the observations that for two numerical simulations having the same value of Δ, that for which $\gamma < 0$ has a faster rate of instability than the solution with $\gamma > 0$.

If $|\Delta_m| \gg |\Delta|$, then the solution will be dominated by a solitary wave instability where the trapped mode has $k \approx (\Delta/3)^{1/2}$ either upstream or downstream. We refer to Figure 12. In the case of a plateau upstream and a trough downstream, the downstream caustic for the most unstable mode is now at finite distance downstream from the topographic maximum; however, the upstream caustic remains far upstream. As evidence suggests this is the dominant caustic, the instability remains the same for the case of a localized solution though the rate of growth of this instability is slower. For a plateau downstream and trough upstream, the upstream caustic is now a finite distance from the topographic maximum and consequently the growth mode of the instability is enhanced.
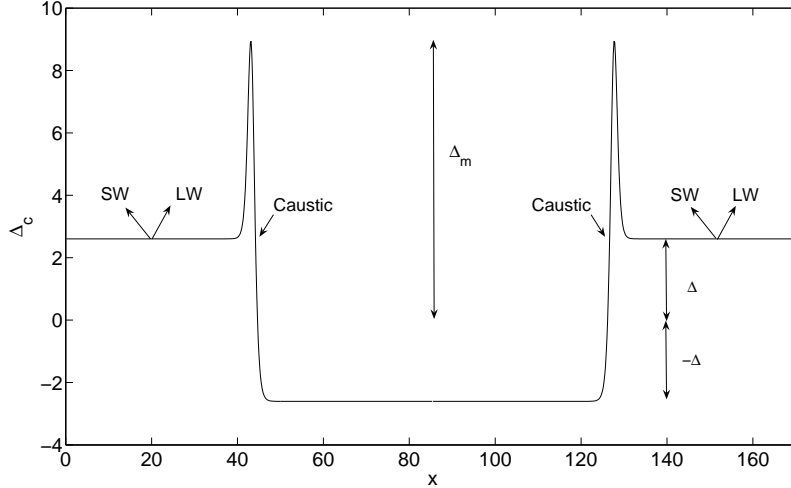
Fig. 12. A sketch of the scaled velocity perturbation for a periodic dispersive hydraulic solution of (1) using $\gamma = -3.85$, $\Delta = 2.604$. Caustic locations and directions of short (SW) and long (LW) wave propagation for the slowly varying theory are shown. Δ_m is the maximum of Δ_c over the domain.

4 Conclusion

The goal of this paper has been to characterize the nonlinear stability of steady weakly dispersive hydraulic solutions of the fKdV equation. This has been investigated using direct observations of integral properties of the instabilities. The latter has proved to be particularly useful, in that it allows the source of instability to be isolated to the upward and downward jumps which comprise the periodic solutions.

The hydraulic solutions can be characterized in terms of the normalized forcing parameter γ. In terms of this parameter value, the nonlinear stability can be divided into two main categories as shown in Figure 10. Solitary wave instability occurs when the upward and downward solutions are largely symmetric. Consequently the form of the instability at the upstream and downstream solutions is primarily identical. This instability is characterized by the periodic generation of upstream propagating solitary waves and downstream propagating dispersive waves. In both the original and reflected regions, sub-exponential nonlinear growth in the momentum of the perturbation variable occurs prior to saturation.

For solitary type instability problems the source of instabilities is on the downstream flank of the topographic perturbations. In contrast for hydraulic instability, the primary instability only occurs at the downward jump and is characterized by the source of instabilities being on the upstream flank of the topographic perturbation. Prior to saturation, the nonlinear effects serve to accelerate the growth of the perturbation momentum, resulting in super-

20

exponential growth prior to saturation. Like solitary wave instability, the result is the upstream propagation of solitary waves and the downstream propagation of nonlinear wave groups. However in this case, the amplitude is significantly larger. At the upward jump, primary instabilities can occur for non-monotonic jumps in the form of a slower solitary wave type instability.

Thus stable weakly dispersive hydraulic solutions can only occur for $\gamma > 0$ and only for upward jumps. Our numerical simulations indicate that for $\gamma > 0$, the corresponding downward jump experiences a hydraulic type instability. While for $\gamma < 0$, both the upward and downward jumps are nonlinearly unstable. For $|\gamma| \gg 1$, this is a solitary wave instability, while for $|\gamma| \sim 1$ a mixed instability occurs where the downward jump is destabilized by hydraulic instability and the upward jump by solitary wave instability.

The general results detailed here have also been confirmed by separating the upstream and downstream regions using viscous sponge layers. In this circumstance secondary instabilities cannot form due to solitary waves and wave packets generated in one region being able to propagate into the other region. However, other problems such as upstream influence are introduced when the waves reach the sponge layers.

Finally, the employment of wave kinematics was found to be useful in three ways: explaining the source of instabilities, the sub-exponential and super-exponential growth rates and extensions from a finite domain to an infinite domain. The latter is helpful in extending the study to single hydraulic transitions rather than the periodic solutions considered here. It is anticipated that the former two will allow the results obtained here to be extended to generalizations of the fKdV equation, for example the addition of cubic nonlinearity.

Here we have only considered asymmetric solutions where the downward jump is a reflection of the upward jump. However as noted in Ee & Clarke [8], periodic dispersive hydraulic solutions can be formed with non-matching pairs of topographic perturbations. For a particular value of Δ up to six possible values of the forcing parameter γ can be utilized to form such a solution. If these topographic perturbations are sufficiently far apart, since a periodic solution must consist of at least one downward jump, we can conclude that such solutions are nonlinearly unstable. However, as the topographic perturbations move closer together, our numerical simulations demonstrate that the onset of instability takes significantly longer. Thus there is the possibility that for small, but finite, separation between the two topographic perturbations that due to the interactions the combined solutions may be stable. The presence of standing waves on the trough connecting the two jumps, as considered by Dias and Vanden Broeck [12], may also lead to stabilization of the solutions.

We can now return to the trivial initial condition for bell-shaped topography

for the fKdV equation as considered by Grimshaw & Smyth [9] and for which the characteristic solutions are shown in Figure 1. For positive γ, our conclusion is that the steady transition which forms in the vicinity of the topographic perturbation is nonlinearly stable and is accurately described by the weakly dispersive hydraulic solutions discussed here and in Ee & Clarke [8]. The solitary waves which form on the upstream flank of the topography and which are described using various modulation theories by Smyth[14] must simply be a result of the incomplete transition from the trivial initial condition. If $\Delta < 0$ the waves are able to completely detach from the upstream flank, however then a wavetrain is attached to the downstream flank. For negative γ, it can be seen that the solution shown in the lower panel of Figure 1 is typical of a solitary wave instability rather than a hydraulic type instability even though $|\gamma|$ is relatively small. Again, the reason for this would seem to be the transition from the trivial initial condition. In this case, the downward jump is the only solution compatible with the small-time solution for the trivial initial condition. However prior to this being able to form, a solitary wave instability develops and subsequently dominates the asymptotic behaviour.

References

[1] S. R. Clarke and R. H. J. Grimshaw, "Resonantly generated internal waves in a contraction", J. Fluid Mech., **274**, 139-161 (1994)

[2] T. R. Akylas, "On the excitation of long nonlinear waves by a moving pressure distribution", J. Fluid Mech., **141**, 455-466 (1984)

[3] S. Cole, "Transient Waves produced by flow past a bump", Wave Motion, **7**, 579-587 (1985)

[4] S. J. Lee and G. T. Yates and T. Y. Wu, "Experiments and analyses of upstream advancing solitary waves by moving disturbances",J. Fluid Mech., **199**, 569-593 (1989)

[5] T. Y. Wu, "Generation of upstream advancing solitons by moving disturbances", J. Fluid Mech., **184**, 75-99 (1987)

[6] W. K. Melville and K. R. Helfrich, "Transcritical two-layer flow over topgraphy", J. Fluid Mech., **178**, 31-52 (1987)

[7] R. H. J. Grimshaw, "Resonant flow of a rotating fluid past an obstacle: The general case", Stud. Appl. Maths, **83**, 249-269 (1990)

[8] B. K. Ee and S. R. Clarke, "Weakly dispersive hydraulic flows in a contraction - Parametric solutions and linear stability", Phys. Fluids, **19**, 056601 (11 pages) (2007)

[9] R. H. J. Grimshaw and N. Smyth, "Resonant flow of stratified fluid over topography", J. Fluid Mech., **169**, 429-464 (1986)

[10] R. Camassa and T. Y. Wu, "Stability of forced steady solitary waves", Phil. Trans. R. Soc. Lond. A, **337**, 429-466 (1991)

[11] R. L. Pego and M. I. Weinstein, "Eigenvalues and instabilities of solitary waves", Phil. Trans. R. Soc. Lond. A, **340**, 47-94 (1992)

[12] F. Dias and J. M. Vanden-Broeck, "Trapped waves between submerged obstacles", J. Fluid Mech., **509**, 93 (2004)

[13] G. B. Whitham, Linear and Nonlinear Waves, Wiley (1999)

[14] N.F. Smyth, "Modulation theory for resonant flow over topography", Proc. Roy. Soc. Lond. A, **409**, 79–97 (1987)